Results in Physics 5 (2015) 273–280

Contents lists available at ScienceDirect

Results in Physics

journal homepage: www.journals.elsevier.com/results-in-physics

A comparative study on low cycle fatigue behaviour of nano and micro Al_2O_3 reinforced AA2014 particulate hybrid composites

R. Senthilkumar [a,*], N. Arunkumar [b], M. Manzoor Hussian [c]

[a] *Dhanalakshmi Srinivasan College of Engineering & Technology, Chennai, India*
[b] *St. Joseph's College of Engineering, Chennai, India*
[c] *Jawaharlal Nehru Technological University, Hyderabad, India*

ARTICLE INFO

Article history:
Received 24 August 2015
Accepted 28 September 2015
Available online 9 October 2015

Keywords:
Aluminium matrix composites
Nano Al_2O_3
Low cycle fatigue
Plastic strain
Fractured surface

ABSTRACT

Aluminium based metal matrix composites have drawn more attraction due to their improved properties in structural applications for the past two decades. The fatigue behaviour of composite materials needs to be studied for their structural applications. In this work, powder metallurgy based aluminium (AA2014) alloy reinforced with micro and nano-sized alumina particles were fabricated and consolidated with the hot extrusion process. The evaluation of mechanical properties in the extruded composite was carried out. This composite was subjected to low cycle fatigue test with a constant strain rate. Scanning Electron Microscope (SEM) and Transmission Electron Microscope (TEM) images were used to evaluate the fatigue behaviour of aluminium-nano composite samples. Enhanced mechanical properties were exhibited by the nano alumina reinforced aluminium composites, when compared to the micron sized alumina reinforced composites. The failure cycle is observed to be higher for the nano alumina reinforced composites when compared with micron sized alumina composites due to a lower order of induced plastic strain.

Introduction

In recent years, aluminium metal matrix composites (AMMCs) attract more attention due to their lightweight property, low coefficient of thermal expansion, machinability, and superior mechanical properties, such as, yield strength (YS), ultimate tensile strength (UTS), and hardness [1,2]. Because of these advantages, the above class of materials was applied in the automotive industries for the production of pistons, cylinder liners, cam shafts, connecting rods, main bearings, brake rotors and callipers, engine pistons, and electronic components [2]. Many techniques have been developed for producing the particulate reinforced AMMCs, such as, powder metallurgy and squeeze casting [3]. Each of the above methods has its own advantages and disadvantages. Even though powder metallurgy is more complicated than casting techniques, it yields a better interface between the reinforcement and matrix alloy and improves mechanical properties of the composite [3,4]. Extensive works have been carried out to evaluate various ceramic particles as the reinforcement materials for AMMCs [5–8]. Therefore, alumina is a suitable choice as reinforcement due to its good mechanical properties and thermodynamic stability with aluminium, and also the absence of any detrimental reaction at high temperature [9]. Composites with either nano-sized or micro-sized particles alone resulted in agglomeration which act as stress concentration sources which eventually reduce the strength of compacted samples [10]. Clustering of nano particles also prevents perfect densification, leading to lower densities [11]. The micro-structural characteristics and mechanical properties of metal matrix composites are strongly influenced by fabrication techniques and particle size of the reinforcing materials [12,13]. Aluminium matrix nano-composites (AMNCs) were reinforced with a particle size less than 100 nm and drew considerable attention in recent years [14]. The structural applications of the AMMCs involve inevitably fatigue and cyclic deformation characteristics due to the fact that, the structural components experience dynamic loading, which results in the occurrence of fatigue failure. Hence, an understanding of fatigue and cyclic deformation behaviour of AMMCs is critical for the design, durability evaluation and life prediction of engineering components [15–20].

In this work a comparative study of low cycle fatigue behaviour of aluminium–alumina composite of weight percentage 90% aluminium alloy (AA2014) and 10% alumina (particle size of 20–50 μm) and aluminium–alumina hybrid composite of weight percentage of 90% aluminium alloy (AA2014) reinforced with 8% alumina (particle size of 20–50 μm) and 2% alumina (particle size

* Corresponding author.
E-mail address: rsk1970@gmail.com (R. Senthilkumar).

http://dx.doi.org/10.1016/j.rinp.2015.09.004
2211-3797/

Table 1
Chemical composition of AA2014.

Elements	Cr	Cu	Fe	Si	Mg	Mn	Ti	Zn	Al
wt.%	0.05	4.45	0.50	0.65	0.80	0.80	0.15	0.25	Bal.

less than 50 nm) is selected based on previous experimental results [12,13].

Experimental procedure

Composite fabrication

In this work, AA2014 aluminium alloy was used as matrix material and its chemical composition is shown in Table 1. Powders of AA2014 alloy constituent elements were prepared using high energy planetary ball milling process up to four hours. Hardened stainless steels balls of diameter 16 mm were employed to mill the starting material. In order to avoid micro aggregation, an intermediate cooling is carried out to increase the heat dissipation from the vials. SEM image (microstructure) of particle morphology of composites with the content of various wt.% of micro and nano Al_2O_3, sintered at 550 °C is shown in Fig. 1. Aluminium particles are of spherical morphology (Fig. 1a), micron sized alumina particles are flake shaped (Fig. 1b) and nano alumina particles are of spherical morphology (Fig. 1c).

The matrix material was blended with the reinforcement material of Al_2O_3 in nano (with average particle size 50 nm) and micron (with average particle size 20–50 µm) sizes with different weight ratios as shown in Table 2. The matrix and reinforced particles were proportionally weighed and mixed by a ball mill for four hours in clockwise and counter clockwise directions. The rotation speed and time of 300 rpm and 15 min were given for each direction with 1 min rest. The ball–powder ratio was kept as 10:1. Milled powder was uniaxially compacted in a universal testing machine with 50 MPa load to obtain cylindrical samples of Φ30 mm × 80 mm height. Zinc stearate was used as a lubricant medium to reduce friction between the die wall and punch. Cold compacted samples were sintered at 550 °C and soaked for 2 h in argon gas atmosphere to avoid oxidation, then cooled in the same furnace. The samples were hot extruded at 550 °C to the size of 13 mm diameter. The extruded composites were subjected to T6 heat-treatment with solutionizing carried out at 502 °C for 30 min and then oil quenched at room temperature.

XRD analysis was carried out to understand the phase formation in the composite materials. SEM microstructural studies were also conducted to evaluate the distribution of reinforcement, and interfacial integrity between matrix and reinforcement. Microhardness measurements were performed on the polished extruded composite samples using a microhardness tester. The tensile properties of the as-extruded composite were determined as per ASTM standard E8/E8M – 09.

Fatigue samples were prepared for a gauge length of 25.4 mm and a gauge diameter of 3 mm. It is machined with the length of the samples parallel to the extrusion direction. The gage section of fatigue samples was ground along the loading direction with silicon carbide (SiC) papers up to a grade of 1000 to remove the machining marks. Strain-controlled, pull–push type fatigue tests were conducted using a computerised closed loop servo hydraulic controlled fatigue testing system equipped with load cell and stroke transducer. Low cycle fatigue (LCF) tests were conducted at a constant strain rate of $1 \times 10^{-2}\ s^{-1}$ and for a strain amplitude

Table 2
AMMCs composition.

Composite	AA2014 (wt.%)	Micron size Al_2O_3 (wt.%)	Nano size Al_2O_3 (wt.%)
Composite-1 (aluminium–alumina)	90	10	0
Composite-2 (aluminium-hybrid)	90	8	2

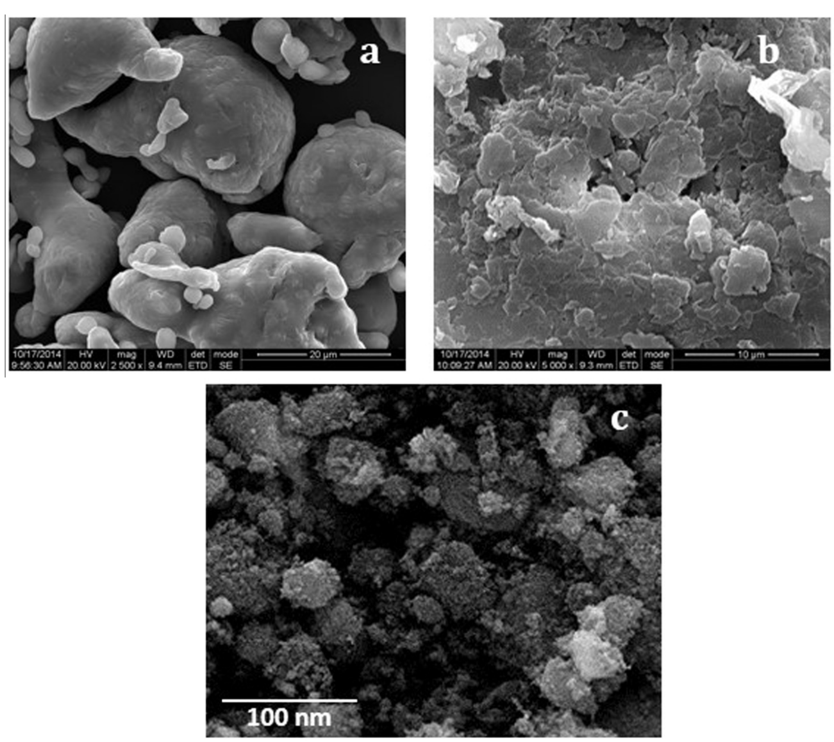

Fig. 1. SEM morphology of (a) aluminium, (b) micron Al_2O_3 and (c) nano Al_2O_3.

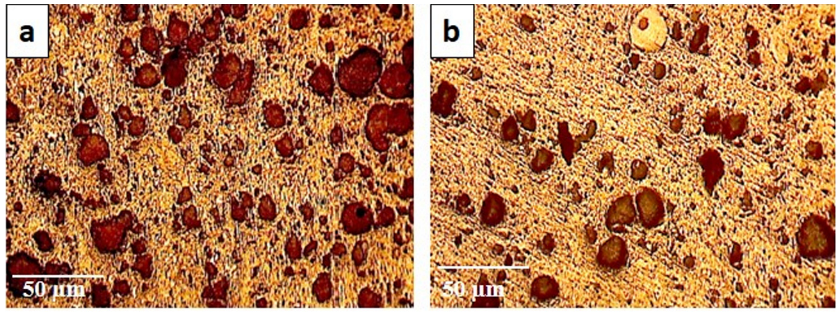

Fig. 2. Optical image of (a) composite-1 and (b) composite-2.

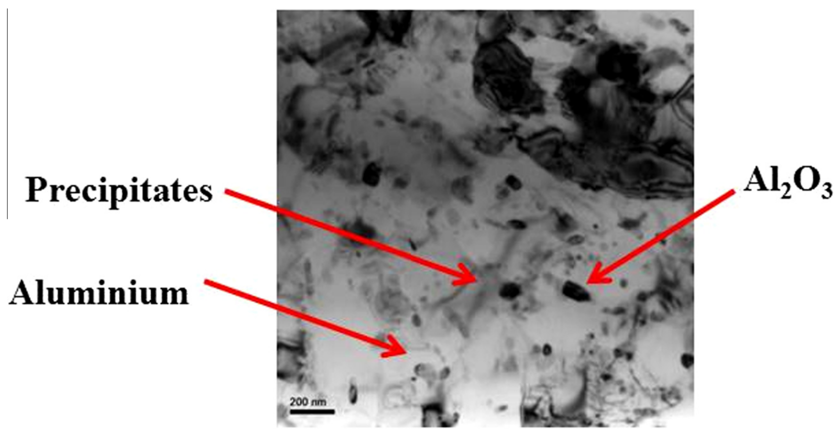

Fig. 3. TEM image of composite-2.

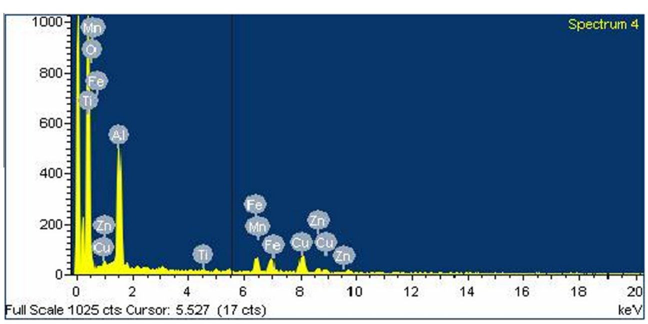

Fig. 4. EDS of composite-1.

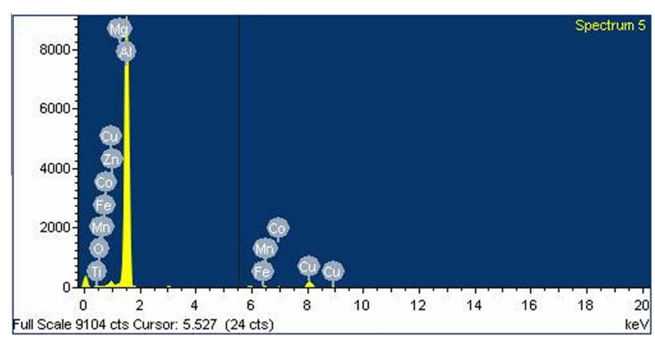

Fig. 5. EDS of composite-2.

of 0.6%, strain ratio $R = -1$ at room temperature (23 °C ± 2 °C). The low-cycle fatigue tests were conducted at total strain amplitudes of 0.1% to 0.6% with step 0.1%. The test results were reported as average of two samples tested at each strain level. Additionally, to study the effect of strain ratio on the LCF behaviour of the composite, tests were also carried out at five different stress ratios of $R = -1$ and 0.3. The fracture surfaces of fatigued specimens were examined via SEM and TEM to identify fatigue crack initiation sites and propagation characteristics.

Results and discussions

Microstructural analysis

Fig. 2 shows the microstructures of the extruded composite-1 and composite-2 in heat treated conditions. As shown in Fig. 2a and b, micron sized alumina particles were dispersed evenly in the AA2014 matrix. Matrix of the composites revealed grains structure by the deep etching at grain boundary and the size and shape of the grains were easily revealed at low magnification optical microscope images. The matrix shows least pores in between the grains that are sintered.

Fig. 3 shows a TEM image of composite-2. This image shows the presence of nano alumina particles. Few sites of clustered nano-alumina were observed. Nano particles around the grain boundary of the matrix material hinder the grain growth and resist the dislocation mobility of grains during loading.

Figs. 4 and 5 show the energy-dispersive X-ray spectroscopy (EDS) images of composite-1 and composite-2. EDS graphs of the above images show the presence of elements such as aluminium (Al), copper (Cu), magnesium (Mg) and silicon (Si) as high intensity peaks and chromium (Cr) and manganese (Mn) as low intensity peaks.

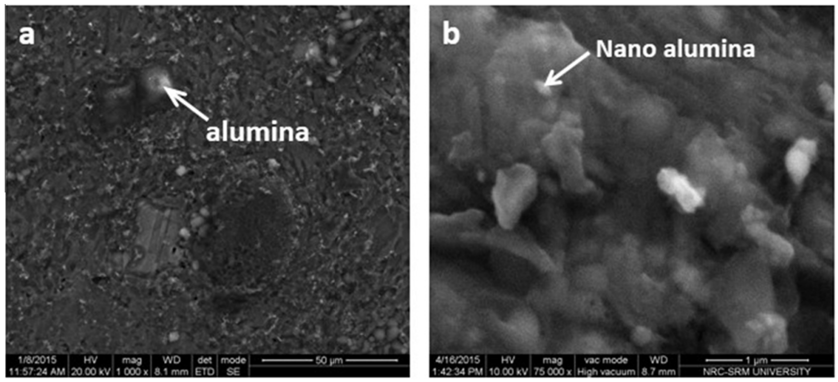

Fig. 6. SEM images of (a) composite-1 and (b) composite-2.

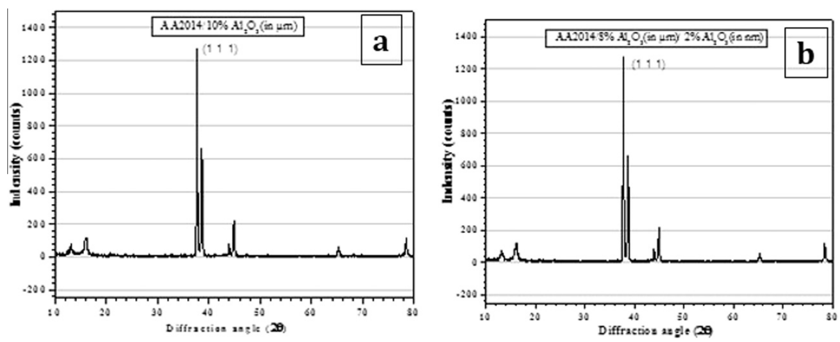

Fig. 7. X-ray diffraction patterns of (a) composite-1 and (b) composite-2.

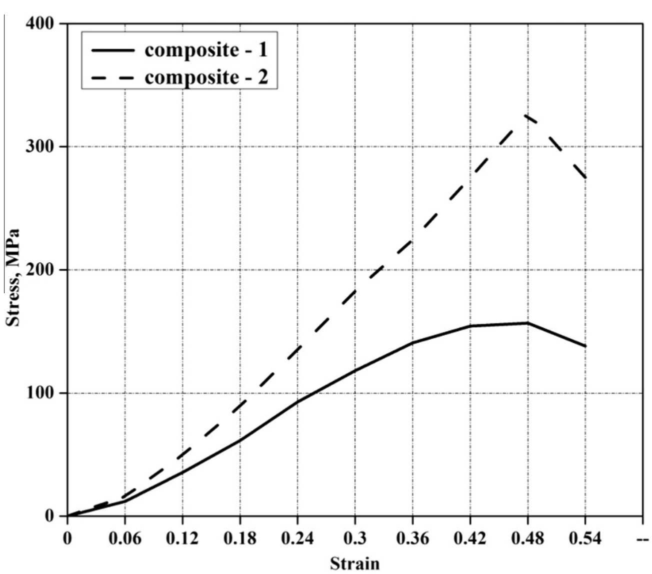

Fig. 8. Compressive strength.

SEM images of composite-1 and composite-2 are shown in Fig. 6. Fig. 6a shows the presence of a precipitate in the heat treated aluminium alloy and exhibits a low order of porosity. Fig. 6b reveals the presence of nano alumina particles and also to get clear visibility of interface between reinforcement particles and matrix, a higher magnification image was presented. This image shows that nano alumina particles dispersed fairly well in the aluminium matrix. A minimal agglomeration of nano alumina particles was also observed in the composite-2. SEM images of the above two composites (Fig. 6) depict the absence of microcracks an indicator of good interfacial strength between the matrix and particles. It is also seen that dispersed phases of precipitate components are in the matrix phase. It was confirmed through an X-ray diffraction (XRD) study. X-ray diffraction patterns obtained from the extruded Al_2O_3/AA2014 composites are shown in Fig. 7. In addition to AA2014 and Al_2O_3 peaks in both samples, Al_2CuMg peaks were also detected in the heat treated composites. This indicates that precipitates were formed during the heat-treatment process. The presence of Al_2CuMg, Mn_3Si and Mg_2Si was reported in the earlier process of similar aluminium matrix composites. Fig. 7 shows XRD images of composite-1 and composite-2. The image also shows the segregated and un-dissolved particles of Cu–Al_2. It is probably due to incomplete dissolution during the sintering process.

Table 3
Mechanical characteristics.

Composites	Micro-hardness (HV)		Compressive strength (MPa)		Yield strength (MPa)	% Elongation	Ultimate tensile strength (MPa)
	Sintered	Extruded	Sintered	Extruded			
Composite-1	45	65	98	157	202	2.87	224
Composite-2	65	98	285	327	255	3.33	264

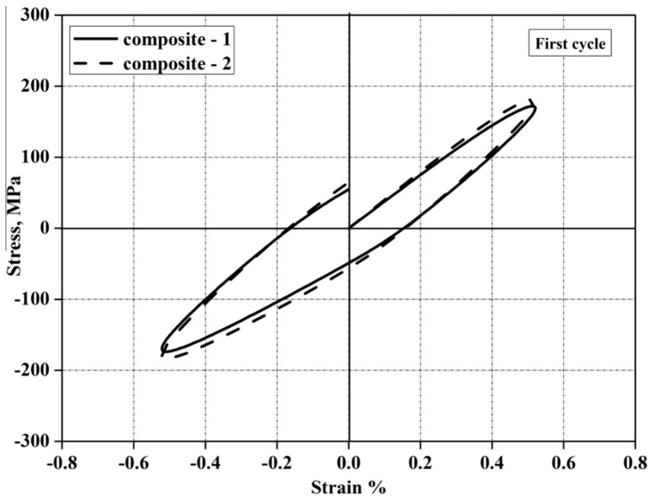

Fig. 9. Hysteresis loop curve at first cycle for composite-1 and composite-2.

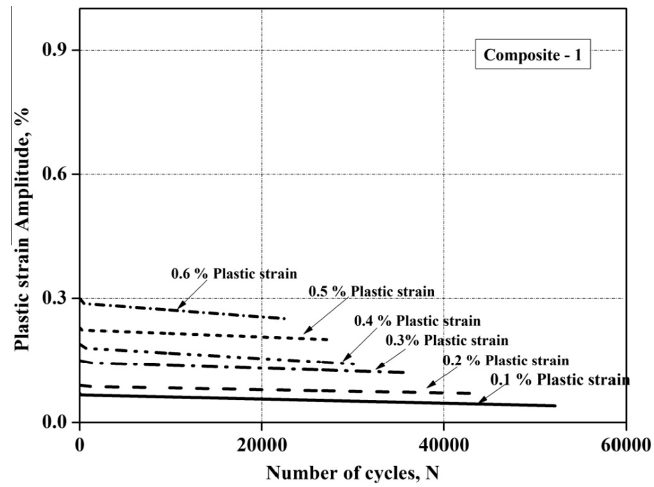

Fig. 12. Plastic strain amplitude vs. number of cyclic deformation composite-1.

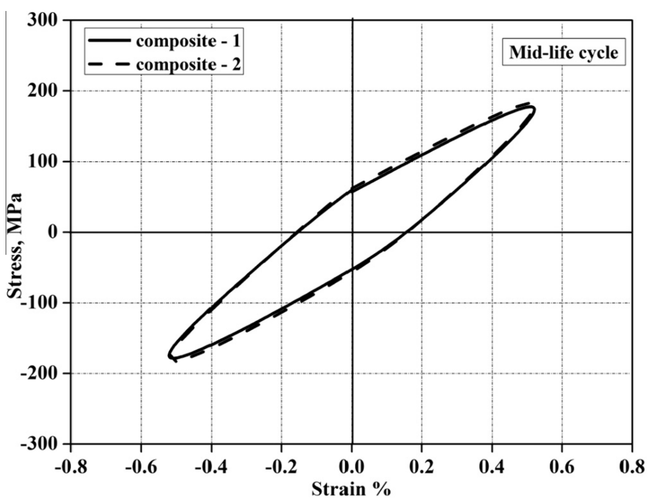

Fig. 10. Hysteresis loop curve at midlife for composite-1 and composite-2.

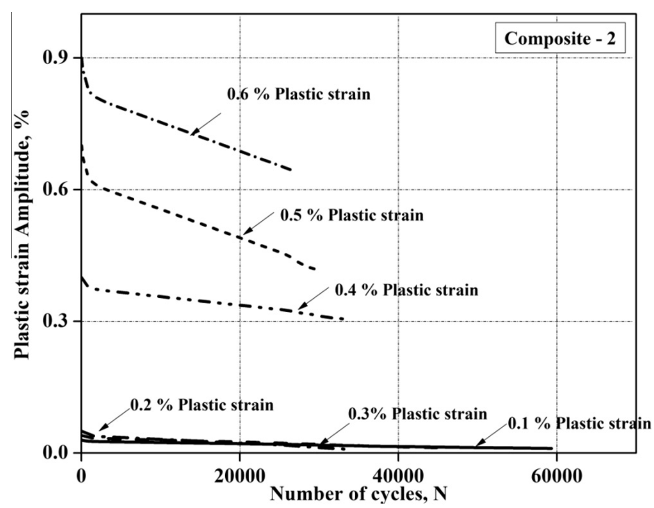

Fig. 13. Plastic strain amplitude vs. number of cyclic deformation composite-2.

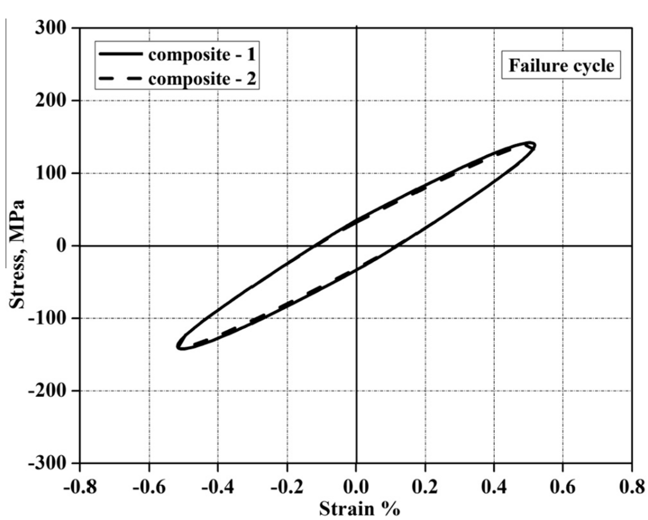

Fig. 11. Hysteresis loop curve at failure cycle for composite-1 and composite-2.

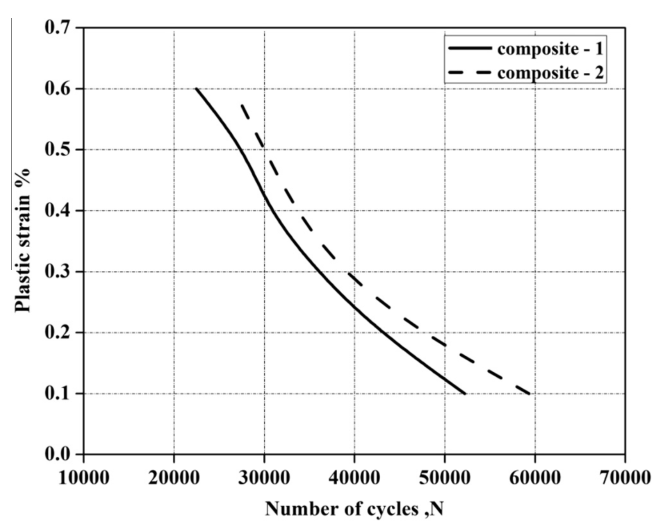

Fig. 14. S–N curve.

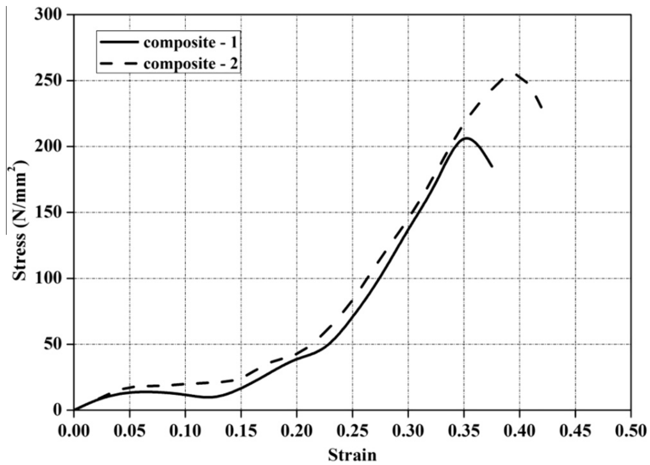

Fig. 15. Monatomic stress–strain curve.

Mechanical properties

In order to understand the mechanical properties, compression tests were conducted at room temperature under uni-axial compressive loading and the stress–strain curves are shown in Fig. 8. Table 3 shows the mechanical properties of composite-1 and composite-2 which clearly indicate that yield and ultimate tensile strength of the composite-2 is higher than that of composite-1. Compression strength values show that the composite-2 has significantly higher values than composite-1 due to the nano Al_2O_3 particles, which can strongly increase the reinforcement efficiency.

Fatigue life of the hybrid and mono reinforcement composites

Fig. 9 shows typical stress–strain hysteresis loops of the first cycles at a given strain amplitude of 0.6% and strain ratio of $R = -1$ for the composites-1 and 2. Asymmetrical hysteresis loops were observed for both the composite-1 and composite-2 as shown

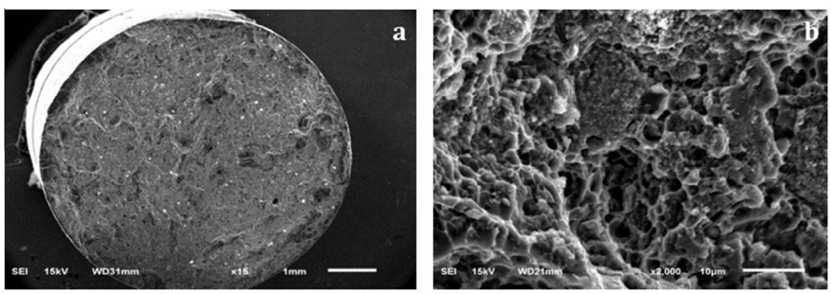

Fig. 16. Fatigue tested composite-1 (a) fractured surface, (b) crack initiation site.

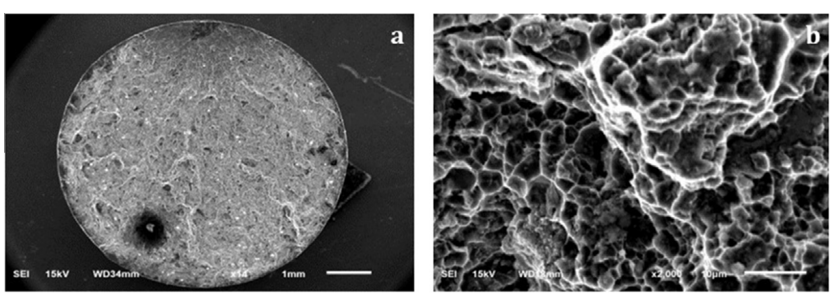

Fig. 17. Fatigue tested composite-2 (a) fractured surface, (b) crack initiation site.

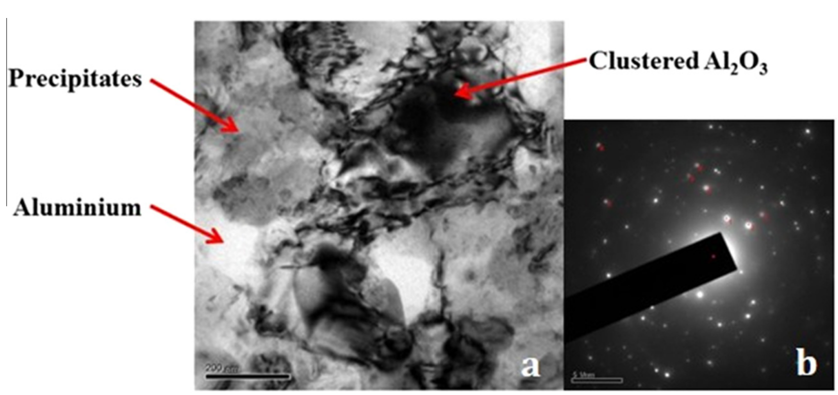

Fig. 18. TEM image of composite-1 (a) fractured surface, (b) SAD pattern.

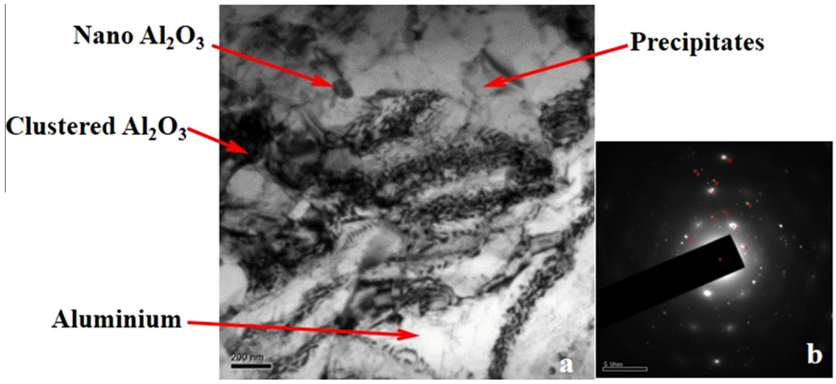

Fig. 19. TEM image of composite-2 (a) fractured surface, (b) SAD pattern.

in the Fig. 9 which confirms the isotropic behaviour of both composites. This observation is in good agreement with the findings of Luk et al. (2015) [17], who reported the hysteresis behaviour of Al-SiC particulate composites. The above phenomenon can be attributed to the dislocation slip-dominated deformations a result of tension–compression deformation because aluminium is a matrix material whose structure is face-centred cubic. Similar symmetrical behaviour was reported in other FCC metals such as SiC_p/2124 [15].

Figs. 10 and 11 show typical stress–strain hysteresis loops of the mid life and failure life cycles at a given strain amplitude of 0.6% and strain ratio of $R = -1$ for the composite-1 and composite-2. It shows that both the composites exhibited symmetrical hysteresis loops at mid-life and failure life. However, there is slight fall in the maximum stress due to those initially reinforced hardened materials.

Variation of the plastic strain amplitude versus the number of cyclic deformation is shown in Fig. 12 for composite-1 with different strain amplitudes. With 0.6% strain amplitude, Al–alumina composite shows the decrease in the plastic strain amplitude with cyclic strain. This is a result of cyclic hardening of successive cycle deformations. Al-alumina composite shows a stable plastic strain for the cyclic deformation at the strain amplitude from 0.1% to 0.5%.

Variation of the plastic strain amplitude versus number of cyclic deformation is shown in Fig. 13 for composite-2 with different strain amplitudes. It is observed from Fig. 12, that plastic strain decreased with the increasing level of cyclic deformation at higher strain amplitude from 0.4% to 0.6%. This indicated that cyclic hardening occurred during the cyclic deformation. At lower strain amplitude, the plastic strain is very gradually decreased with cyclic deformation and remained constant throughout cyclic deformation. This intuitionally showed that initial cyclic hardening occurred with cyclic deformation and then started with stable softening nature.

The cyclic hardening at higher strain amplitude in composite-1, which indicated that the decrease of plastic strain was of low order when compared to the composite-2 (Figs. 12 and 13). A marginal decrease in plastic strain is observed at lower stress amplitude.

In order to understand the fatigue life of the composite-1 and composite-2 S–N curves with total strain amplitudes vs. number of cycle to failure (N_f) were drawn as shown in Fig. 14. Composite-2 exhibited a higher fatigue life when compared to the composite-1 due to nano sized alumina reinforcement which more effectively pinned down the dislocations. A smaller percentage addition of nano sized alumina particles increased the fatigue life to a greater extent. This can be clearly confirmed by observing the monatomic stress–strain curve as seen in Fig. 15. It shows the monatomic stress–strain of composite-1 and composite-2. It is understood that composite-2 exhibited a higher ultimate yield strength than composite-1.

Fractography

Fig. 16a and b shows that fracture surfaces of the composite-1 fatigue tested at a total strain amplitude of 0.6%. Fig. 16a shows lower magnification of the fractured surface of the fatigue tested specimen. Crack initiation, near crack initiation site and fast facture surface were clearly observed. Fig. 16b shows the occurrence of fracture surface with limited dimple structure and more reinforcement particles. It indicates the presence of a stronger matrix and reinforcement interface.

Fig. 17a and b show the fracture surfaces of fatigue tested composite-2 at a total strain amplitude of 0.6%. Fig. 17a shows a fatigue crack initiation from the specimen surface. The crack growth near the initiation site occurred primarily in the matrix phase material. It could also be observed that there is no particle and matrix interface cracking or reinforcement particle cracking, and a fast fracture site was also clearly observed. Fig. 17b shows that fracture surfaces were of dimple morphology and mixed mode fractures such as the limited flat region and the particle decohesion of nano sized alumina particles was also observed.

It is also understood that dimple density of the composite-2 is higher than that of the composite-1. However, fracture surface observations were similar to the composite-2, except the occurrence of more alumina particle cracking.

TEM images of the fractured surface of composite-1 are shown in Fig. 18a and b. Fig. 18a shows the presence of alumina particles and the occurrence of cracking due to higher interfacial strength between aluminium and alumina particles. There is no evidence of interfacial products in the above image. Dislocation that started from aluminium grains ended with adjacent alumina particles, can be observed. From the above image precipitates of aluminium alloys restrict the movement of dislocation and tend to increase the internal plastic strain of the composite. Fig. 18b shows the TEM image of fractured surface composite-1 with the SAD pattern. Alumina particles cracking with strong interface were observed from Fig. 18a. Bright spot of the SAD pattern (Fig. 18b) clearly indicated the formation of precipitates such as Mg, Al_2Cu, Mg and Cu–Al_2. Alumina particles are indicated at the bright spot of the diffused light area.

TEM images with the SAD pattern of the fractured surface of composite-2 are shown in Fig. 19a and b. Fig. 19a shows the presence of nano alumina and clustered nano alumina and alumina particles in the aluminium matrix. The precipitates alloying elements Cu, Mg and Zn resulted more dislocation of pinning site and thereby a higher dislocation density. The inset in the Fig. 19b represents the selected SAD pattern with continuous rings, which confirms the nano-crystalline nature of the composite powder. The bright areas in the micrograph correspond to nano-sized reinforcement crystallites.

The crystallite size calculated from X-ray peak broadening and the absence of other peaks indicating no formation of intermetallic layer are in close agreement with that of HRTEM observations strong bonding between CNTs and nano particles, denser dislocation tangles can be observed from the TEM image (Fig. 19a).

Conclusions

Low cycle fatigue tests were conducted on extruded AA2014-micro sized alumina (composite-1) and AA2014-micro-nano alumina (composite-2) composites at varying strain amplitudes with zero strain ratio. The following conclusions are drawn from this investigation.

1. Microstructure study showed the uniform distribution of alumina particles in the extruded composite-1. In the case of composite-2, TEM images revealed the presence of nano alumina particles fairly distributed in the aluminium matrix with some site clustering of alumina nano particles. TEM studies also confirmed the presence of dominated precipitates distributed in the metal matrix.
2. Composite-2 exhibited higher mechanical properties such as yield strength and ultimate tensile strength than composite-1.
3. Low cycle fatigue tested composite-2 resulted in symmetrical hysteresis loop in the tension and compression states, which clearly reflected the isotropic material behaviour and slip dominated plastic deformation.
4. Composite-2 exhibited that cyclic plastic strain decreased with increasing amount of cyclic deformation at a higher strain amplitude from 0.4% to 0.6% due to the occurrence of cyclic hardening while deformation continued. Hence the plastic strain gradually decreased with the cyclic deformation and stabilized its value over the entire cycle. Composite-1 showed the stable plastic strain over the entire cyclic deformation at all ranges of strain amplitude being fatigue tested. The cyclic hardening of composite-1 showed the short cycle deformation when compared to the composite-2 which indicates the decrease of plastic strain at low order when compared to composite-2.
5. Composite-2 exhibited a higher fatigue life when compared to the composite-1 due to nano sized alumina reinforcement which more effectively, restricted the dislocation mobility. It is clear evidence that a smaller percentage addition of nano sized alumina particles increased the fatigue life to a greater extent.
6. Fractured surfaces of the composite-2 with total strain amplitude of 0.6% showed that crack formation from the surface and crack growth near the initiation site can occur primarily in the matrix phase material.
7. TEM results confirm that, micron size alumina reinforced particles were cracked and nano particles have pinned down the dislocation.

References

[1] Baghchesara MA, Abdizadeh H. Microstructural and mechanical properties of nanometric magnesium oxide particulate-reinforced aluminium matrix composites produced by powder metallurgy method. J Mech Sci Technol 2012;26(2):367–72.

[2] Valibeygloo N, Khosroshahi RA, Mousavian RT. Microstructural and mechanical properties of Al-4.5wt% Cu-reinforced with alumina nanoparticles by stir casting method. Int J Miner Metall Mater 2013;20(10):978.

[3] Yar A, Montazerian M, Abdizadeh H, Baharvandi HR. Microstructure and mechanical properties of aluminum alloy matrix composite reinforced with nano-particle MgO. J Alloys Compd 2009;484(1–2):400–4.

[4] Wang HJ, Jin ZH, Miyamoto Y. Effect of Al_2O_3 on mechanical properties of Ti_3SiC_2/Al_2O_3 composite. J Ceram Int 2002;28:931–4.

[5] Patel A, Das S, Prasad BK. Hot deformation behaviour of AA2014–10 wt% SiC composite. Trans Indian Inst Met 2014;67(4):521–30.

[6] Rostamzadeh T, Shahverdi HR. Microstructure study on Al-5% SiC nanocomposite powders. Iran J Mater Sci Eng 2011;8(1):32–9.

[7] Atïk E. Mechanical properties and wear strengths in aluminium-alumina composites. Mater Struct 1998;31(6):418–22.

[8] Ansary Yar A, Montazerian M, Abdizadeh H, Baharvandi HR. Microstructure and mechanical properties of aluminium alloy matrix composite reinforced with nano-particle MgO. J Alloys Compd 2009;484:400–4.

[9] Kok M. Production and mechanical properties of Al_2O_3 particle-reinforced 2024 aluminium alloy composites. J Mater Process Technol 2005;161:381–7.

[10] Atrian, Majzoobi GH, Enayati MH, Bakhtiari H. Mechanical and microstructural characterization of Al7075/SiC nanocomposites fabricated by dynamic compaction. Int J Miner Metall Mater 2014;21(3):295–303.

[11] Ramesh CS, Hirianiah A. A review on hot extrusion of metal matrix composites. Int J Eng Sci 2012;1:30–5.

[12] Senthilkumar R, Arunkumar N, Manzoor Hussian M, Vijayaraj R. Study of microstructure and mechanical properties of sintered aluminum alloy composite reinforced with nanoparticles. Adv Mater Res 2014;849:62–8.

[13] Senthilkumar R, Arunkumar N, Hussian NM. Study of microstructure and mechanical properties of sintered aluminum alloy composite reinforced with Al_2O_3 nano particles. Appl Mech Mater 2015;3:6–12.

[14] Mazahery A, Alizadeh M, Shabani MO. Study of Tribological and mechanical properties of A356-nano SiC composites. Trans Indian Inst Met 2012;65 (4):393–8.

[15] Ding HZ, Biermann H, Hartmann O. Low cycle fatigue crack growth and life prediction of short-fibre reinforced aluminium matrix composites. Int J Fatigue 2003;25(3):209–20.

[16] Fouret C, Degallaix S. Experimental and numerical study of the low-cycle fatigue behaviour of a cast metal matrix composite Al-SiC_p. Int J Fatigue 2002;24:223–32.

[17] Luk MJ, Mirza FA, Chen DL, Ni DR, Xiao BL, Ma ZY. Low cycle fatigue of SiC_p reinforced AA2009 composites. Mater Des 2015;66:274–83.

[18] Harik VM, Klinger JR, Bogetti TA. Low-cycle fatigue of unidirectional composites: bi-linear S–N curves. Int J Fatigue 2002;24:455–62.

[19] Ding HZ, Biermann H, Hartmann O. Low cycle fatigue crack growth and life prediction of short-fibre reinforced aluminium matrix composites. Int J Fatigue 2003;25:209–20.

[20] Bekheet N, Gadelrab R, Salah M, Abd El-Azim A. The effects of aging on the hardness and fatigue behavior of 2024 Al alloy/SiC composites. Mater Des 2002;23(2):153–9.